Characterization of Active Sites over Reduced Ni−Mo/Al_2O_3 Catalysts for Hydrogenation of Linear Aldehydes

Xueqin Wang and Umit S. Ozkan*

Department of Chemical Engineering, The Ohio State University, 140 West 19th Avenue, Columbus, Ohio 43210

Received: August 4, 2004; In Final Form: October 14, 2004

Reduced Ni−Mo/Al_2O_3 catalysts exhibit a behavior analogous to that of sulfided Ni−Mo/Al_2O_3 catalysts in hydrogenation of linear aldehydes to alcohols. Similar to what has been previously reported for sulfided catalysts, NO and CO_2 can be used over the reduced Ni−Mo catalysts as probe molecules for the active sites responsible for two competing reactions—aldehyde hydrogenation to alcohols and condensation reactions to heavy products, respectively. Reduced catalysts have a higher aldehyde conversion activity and alcohol selectivity than their sulfided counterparts. The reduction temperature has a strong effect on the surface density of anion vacancies, which are responsible for alcohol formation. Reduction temperature also plays a role in determining the abundance of OH groups on the alumina surface. The effect of reduction temperature also manifests itself through the differences seen in the oxidation states of Mo and Ni species.

1. Introduction

Mo catalysts supported on Al_2O_3 are studied extensively in many hydrotreating processes, including hydrodesulfurization (HDS), hydrodenitrogenation (HDN), hydrodeoxygenation (HDO), and hydrogenation (HYD). In these catalysts, Ni and Co compounds are generally used as promoters. According to a widely accepted model by Topsøe and co-workers, sulfidation of the oxide phase results in the formation of stacks of MoS_2 slabs over the support surface and the Ni and Co species are located primarily on the edges of these stacks.[1−4] Active-site models based on these structures have been used to account for different product distributions observed in HDS, HDN, and HDO reactions.[5−15] Several of these studies have assigned the hydrogenation activity to coordinatively unsaturated sites (CUS), that is, sulfur vacancies associated with Ni and Mo centers, and the hydrogenolysis activity to Bronsted acid sites neighboring sulfhydryl groups. It was also proposed that reduced Ni−Mo/Al_2O_3 catalysts might exhibit similar activity where OH groups act in a manner analogous to that of SH groups and anion vacancies (CUS) can form during reduction process as well.[16−18] Although the relationships between different active sites, such as coordinatively unsaturated sites (CUS), Brønsted acid sites, SH and OH groups, over sulfided Ni−Mo and Co−Mo catalysts and different reaction steps in HDS, HDN, and HDO reactions are studied extensively, similar correlations in aldehyde hydrogenation reactions have not been the focus of many studies. In our previous articles,[19−22] we have reported on the catalytic performance of sulfided Ni−Mo/Al_2O_3 catalysts in the hydrogenation of linear aldehydes to alcohols. The two primary reactions that are of most interest in these reaction schemes are (1) the hydrogenation of the aldehyde to form a corresponding alcohol, that is, the desired reaction, and (2) the formation of heavy products through reactions such as aldol condensation of aldehydes and condensation of aldehydes with alcohols, that is, the undesired reactions. We have also shown that NO and CO_2 could be used as molecules to probe the active sites that promote the hydrogenation and heavy-product formation reactions, respectively, as the alcohol formation is correlated to CUS density while the heavy-product formation could best be explained by the surface concentration of OH and possibly SH groups.

In this article, we present the results of our studies on the effect of reduction temperatures on oxidation states of Mo and Ni species on reduced Ni−Mo/Al_2O_3 bimetallic catalysts and, in turn, on active-site density. The catalyst sulfided at 400 °C was included in this study for comparison. It appears that pretreatment conditions have a strong effect in determining the surface density of various species with different oxidation states and the active sites for NO and CO_2 adsorption over the bimetallic Ni−Mo/Al_2O_3 catalysts. Catalysts that have been exposed to different pretreatment conditions have been characterized using in-situ X-ray diffraction (XRD), X-ray photoelectron spectroscopy (XPS), diffuse reflectance infrared Fourier transform spectroscopy (DRIFTS), temperature-programmed desorption (TPD), and volumetric chemisorption measurement techniques. Catalyst performance with regard to activity and product distribution has been studied using two different linear aldehydes—hexanal and propanal.

2. Experimental Section

Alumina-supported catalysts with 15% MoO_3 and 3% NiO loadings were prepared by wet co-impregnation of γ-Al_2O_3 with aqueous solutions of ammonium heptamolybdate and nickel nitrate. The preparation procedure was presented previously.[19,23,24] The surface area of oxidic sample (188 m^2/g) was measured using the BET method with a Micromeritics ASAP2010 automatically controlled instrument, using nitrogen as adsorbent at liquid nitrogen temperature (−196 °C). The catalysts to which we refer in this article are all calcined at 500 °C under oxygen before undergoing any sulfidation or reduction pretreatment step. The nomenclature used in naming the catalysts on the basis of the way they are pretreated is presented in Table 1.

* Author to whom correspondence should be addressed. Phone: (614)-292-6623. Fax: (614)-292-9615. E-mail: Ozkan.1@osu.edu.

10.1021/jp046489q CCC: $30.25
Published on Web 01/14/2005

TABLE 1: Nomenclature Used in Naming the Catalysts

nomenclature	description
O-500	Ni−Mo/Al_2O_3 catalyst calcined at 500 °C for 4 h with O_2
O-NiO-500	NiO sample calcined at 500 °C for 4 h with O_2
O-Ni$(NO_3)_2$-500	Ni$(NO_3)_2$ sample calcined at 500 °C for 4 h with O_2
S-400	Ni−Mo/Al_2O_3 catalyst sulfided at 400 °C for 10 h with 10% H_2S in H_2
S-400-He-500	Ni−Mo/Al_2O_3 catalyst sulfided at 400 °C for 10 h with 10% H_2S in H_2 following He flushing for 2 h at 500 °C
S-Al_2O_3	Al_2O_3 support sulfided at 400 °C for 10 h with 10% H_2S in H_2
R-T	Ni−Mo/Al_2O_3 catalyst reduced at temperature *T* (°C) for 10 h with H_2
R-Al_2O_3-500	Al_2O_3 support reduced at 500 °C for 10 h with H_2
R-NiO-500	NiO sample reduced at 500 °C for 10 h with H_2
R-$NiMoO_4$-500	$NiMoO_4$ sample reduced at 500 °C for 10 h with H_2

XRD Studies. In-situ X-ray powder diffraction (XRD) patterns were acquired by a Bruker D8 Advance X-ray diffractometer equipped with atmosphere- and temperature-control capabilities (cryogenic to 1200 °C) and operated at 40 kV and 50 mA. The powder diffraction patterns were recorded in the 2θ range from 20 to 80°. Reduction was performed in-situ under 5% H_2/N_2 gas flow using a linear temperature-program between isothermal steps. The catalysts were kept at isothermal steps for 0.5 h, and the ramp rate between the isothermal steps was 10 °C/ min.

XPS Studies. X-ray photoelectron spectroscopy analysis (XPS) was performed using an AXIS Ultra XPS spectrometer, operated at 13 kV and 10 mA with monochromator Al Kα radiation (1486.6 eV). Reduced and sulfided catalysts were mounted on a sample holder with conductive tape in a dry glovebox filled with Ar. The sample holder was then transferred to the analysis chamber of the spectrometer with a controlled-atmosphere transporter. Charge neutralization was used to reduce the effect of charge built on samples. All binding energies were referenced to Al 2p of 74.4 eV.

DRIFTS Studies. Diffuse reflectance infrared Fourier transform spectroscopy (DRIFTS) experiments were performed using a Bruker IFS66 instrument equipped with DTGS and MCT detectors and a KBr beam splitter. The catalyst was placed in a sample cup inside a Spectratech diffuse reflectance cell equipped with KBr windows and a thermocouple mount that allowed direct measurement of the surface temperature. Spectra for each experiment were averaged over 1000 scans in the mid-IR range (400−4000 cm^{-1}) to a nominal 3 cm^{-1} resolution. After in-situ pretreatment of the samples with H_2 or He at the desired temperature for 1 h, the temperature was decreased to the adsorption temperature used for different experiments and the background spectra were taken under He flow. The adsorption process for NO and CO_2 was carried out by introducing NO (5450 ppm in He) or CO_2 into the system at room temperature for 1 h. After adsorption, the system was subsequently purged for 1 h with He at a flow rate of 30 cm^3/min. The spectra were collected under He flow, and the background spectrum was subtracted from the post-adsorption spectra. Pyridine was carried into the chamber by He with a diffusion tube for 20 min, followed by flushing with He for 1.0 h. The spectra were collected with an MCT detector, which was operated at −196 °C.

Volumetric Measurement of Adsorbed Probe Molecules. The volumetric measurements of CO_2 and NO chemisorptions (at 30 and −78 °C, respectively) were performed using a Micromeritics ASAP2010 instrument. Before chemisorption measurements, the catalysts were pretreated in-situ at the same conditions as those used prior to reaction in the reactor. An adsorption isotherm, which represents the amount of gas adsorbed as a function of pressure, was obtained. After the first adsorption isotherm was completed, the system was evacuated for 1 h at 10^{-5} Torr. Then, a second adsorption isotherm was obtained. The amount of probe molecule chemisorbed was obtained by calculating the difference between the two isothermal adsorption amounts.

Propanal TPD Studies. TPD experiments were performed using a system previously described.[25] The reactor effluent composition was continually monitored as a function of sample temperature by a mass spectrometer (Hewlett-Packard, MS Engine 5989A). For each of the TPD runs, 150 mg of sample was loaded in a quartz reactor. All samples were reduced or sulfided in-situ using the same procedure as in reaction studies followed by He flushing for 2 h at the designated temperature and cooled to 30 °C in He flow. Propanal adsorption was performed at 30 °C for 1.5 h by introducing propanal through a diffusion tube using a 30 cm^3 (STP)/min He flow at room temperature. After being flushed with He for 2 h at the same temperature, the samples were heated at a rate of 10 °C/min under a 30 cm^3 (STP)/min He flow.

Reaction Studies. The reaction studies of hydrogenation of hexanal and propanal were carried out in a fixed-bed reactor system, which is described in previous articles.[19,20] Prior to reaction studies, the catalysts were reduced or sulfided in-situ. Reduction was performed at 500 °C for 10 h with 40 cm^3/min pure H_2. Sulfidation was carried out at 400 °C for 10 h with 40 cm^3/min mixed gas of 10% H_2S in H_2. Reduced or sulfided catalysts were degassed under a He flow for 2 h at reduction or sulfidation temperatures before being cooled to the desired reaction temperature.

3. Results and Discussion

3.1. In-Situ XRD of Ni−Mo/Al_2O_3 Catalysts during Reduction.

The in-situ X-ray diffraction patterns of 3% Ni−15 % Mo/γ-Al_2O_3 sample obtained using the controlled-atmosphere analysis capability of the XRD system are presented in Figure 1. X-ray diffraction patterns are taken in-situ during a stepwise temperature-programmed reduction process where a previously calcined sample is reduced in 5% H_2 in N_2. The major diffraction features observed over the calcined sample are those of the γ-Al_2O_3. There is a very weak feature at a *d*-spacing of 3.35 Å that may correspond to the (hkl = 220) diffraction line from β-$NiMoO_4$,[22] which decreases in intensity with increasing reduction temperature and disappears above 400 °C. Until a reduction temperature of 600 °C is reached, no new phases are observed. When reduced above 600 °C, MoO_2 phase begins to appear with a *d*-spacing of 3.42 Å. There are also diffraction lines at 2.11 Å that appear around the same temperature, that are likely to correspond to a Ni−Mo alloy or a nonstoichiometric phase $Ni_xMo_yO_z$. Above 700 °C, a Mo metallic phase begins to form, as seen through the 2.22-, 1.57-, and 1.28-Å diffraction lines. Also seen above 700 °C is a diffraction feature that represents a $NiAl_2O_4$ phase.

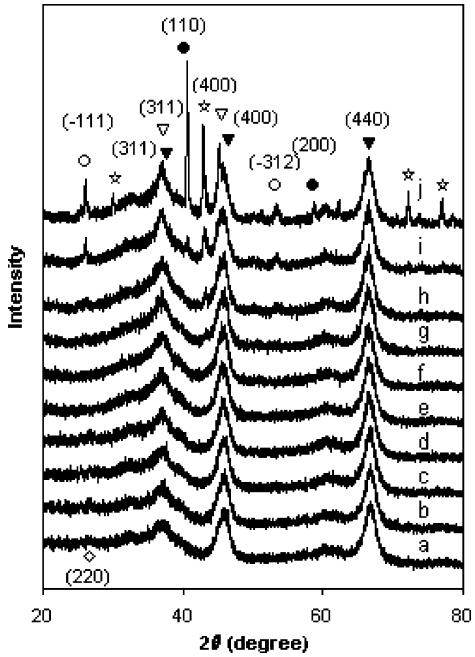

Figure 1. In-situ X-ray diffraction patterns of 3% NiO−15% MoO_3/γ-Al_2O_3 during temperature-programmed reduction. ▼ Al_2O_3, ▽ $NiAl_2O_4$, ◇ β-$NiMoO_4$, ○ MoO_2, ● Mo metal, ☆ Mo−Ni alloy. (a) 30 °C, (b) 150 °C, (c) 300 °C, (d) 400 °C, (e) 500 °C, (f) 600 °C, (g) 650 °C, (h) 700 °C, (i) 750 °C, (j) 800 °C.

3.2. XPS of Ni−Mo/Al_2O_3 Catalysts Reduced at Different Temperatures.

Figure 2 shows the Mo 3d region of the X-ray photoelectron spectra of Ni−Mo/Al_2O_3 catalysts reduced at 400°, 500°, 600°, and 700 °C (R-400, R-500, R-600, R-700). All samples are calcined at 500 °C before being reduced or sulfided. The spectra obtained over the calcined sample (O-500), and the sample that has been sulfided at 400 °C (S-400) are also included for comparison. The spectra were deconvoluted using the constraints of having equal spin−orbit splitting of Mo 3d peaks, the height ratio of $Mo3d_{5/2}$ to $Mo3d_{3/2}$ being constant at 1.5 (theoretical value), and the full width at half-maximum (fwhm) of these peaks being equal. The fwhm remained constant for all Mo oxide species at different oxidation states (+6, +5, +4), except for Mo <+4 for which the fwhm decreased continuously with increasing reduction temperature. The fwhm for MoS_2 species was also different from the Mo oxide species. Percent distribution of different oxidation states for Mo and Ni species obtained through the deconvolution procedure are listed in Table 2.

The XPS spectrum of the oxidized Ni−Mo/Al_2O_3 catalyst shows only Mo^{6+} species with $Mo3d_{5/2}$ and $Mo3d_{3/2}$ binding energies at 233.1 and 236.2 eV, respectively. XPS spectrum of sulfided Ni−Mo/Al_2O_3 catalyst shows Mo to be primarily in the +4 oxidation state with $3d_{5/2}$ and $3d_{3/2}$ binding energies at 228.8 eV and 231.9 eV, respectively. The other prominent feature on the spectrum is the S^{2-} species with a 2s binding energy at 226.2 eV. Deconvolution of the spectrum shows a small amount of Mo^{6+} to be also present (about 8%), which may be due to Mo species in strong interaction with the support, as suggested earlier in the literature.[19,26,27] The fwhm for Mo^{4+} in sulfided catalyst (1.2 eV) is smaller than that of the oxidized (1.8 eV) catalysts. This finding is in agreement with the principle that photoelectron lines of insulating solids are wider than those of conductors,[28] since the sulfidation process transforms the surface Ni and Mo oxide species to Ni and Mo sulfide, which are more conductive. The fact that XPS experiments showed sulfided samples to have a much lower charge shift than oxidized samples is also consistent with this observation. The smaller fwhm for Mo^{4+} may also be related to the crystallinity of MoS_2.

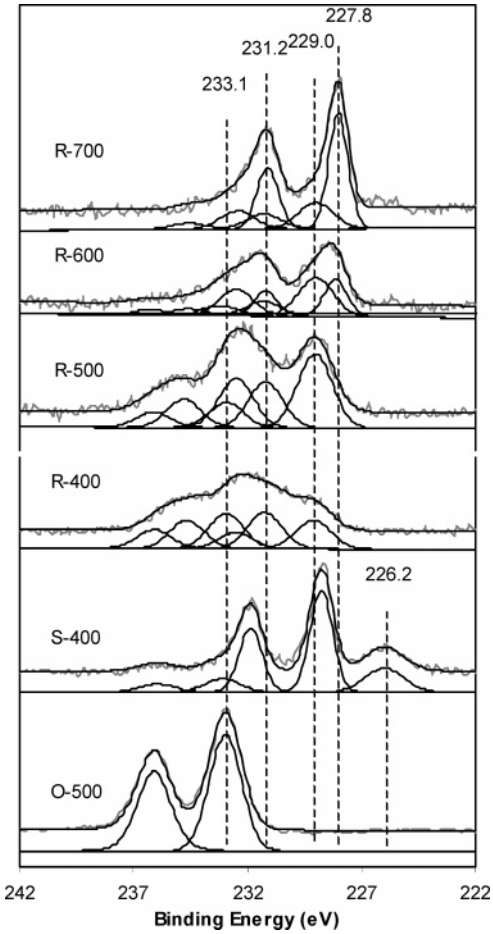

Figure 2. X-ray photoelectron spectra (Mo *3d* - S *2s* region) of Ni−Mo/Al_2O_3 catalysts reduced at different temperatures. Calcined and sulfided samples are included for comparison.

Ni−Mo/Al_2O_3 catalysts reduced at 400 and 500 °C exhibit three Mo oxidation states, with $3d_{5/2}$ binding energies for Mo^{5+} and Mo^{4+} species at 231.2 and 229.0 eV, respectively. The sample reduced at 400 °C has most of the Mo species in the +6 oxidation state (~38%), while reduction at 500 °C makes Mo^{4+} the most prominent species (~51%) (Table 2). The Mo^{4+} binding energies observed over the reduced samples are about 0.2 eV higher than those of the sulfided catalysts. Reduction at 600 °C leads to a broadening of the Mo $3d_{5/2}$ peak with a shift to lower binding energies. The deconvolution shows the emergence of a new peak at a lower binding energy, with $3d_{5/2}$ and $3d_{3/2}$ binding energies at 228.1 and 231.2 eV, respectively. This species is denoted as $Mo^{<4+}$, suggesting an oxidation state lower than +4. The fwhm for these peaks is 1.3 eV, significantly smaller than those seen in oxide phases. After reduction at 700 °C, the Mo^{6+} species disappear altogether and the majority of the Mo species (~64%) appear to be at zero oxidation state, with $3d_{5/2}$ and $3d_{3/2}$ binding energies at 227.8 and 230.9 eV, respectively. The fwhm of these peaks is 1.1 eV, which is, as expected, much lower than those observed over the oxide or the sulfide phases.[28] The presence of Mo metal on Mo/Al_2O_3 catalysts reduced at higher temperatures was reported in the literature previously.[29−33]

Interpretation of the Ni 2p region of the X-ray photoelectron spectra poses some challenges as a result of similar Ni 2p binding energies for different Ni species. To help with the

TABLE 2: Distribution of Mo and Ni Oxidation States in Ni−Mo/Al_2O_3 Catalysts Pretreated at Different Conditions

	Mo species				Ni species		
samples	233.1 eV (Mo^{6+})	231.2 eV (Mo^{5+})	229.0−228.8 eV (Mo^{4+})	228.1−227.8 eV ($Mo^{<4+}$)	856.2 eV (A)	853.5 eV (B)	852.7 eV (C)
O-500	100				100		
S-400	8		92		25	75	
R-400	38	34	28		72		28
R-500	17	31	51		55		45
R-600	12	14	45	29	31		69
R-700		13	23	64	26		74

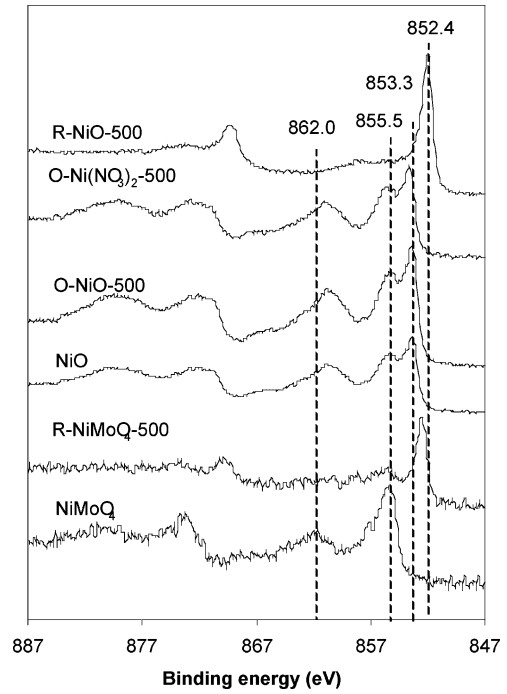

Figure 3. X-ray photoelectron spectra (Ni *2p* region) of NiO, $NiMoO_4$, and $Ni(NO_3)_2$ samples treated at different conditions. Calcined Ni−Mo/Al_2O_3 catalyst is included for comparison.

identification of the Ni species in the catalyst samples, a set of spectra was taken using bulk NiO and $NiMoO_4$ samples for comparison. These spectra are presented in Figure 3. The samples represented in this figure are bulk $NiMoO_4$, bulk $NiMoO_4$ reduced at 500 °C, bulk commercial NiO as received, bulk NiO calcined at 500 °C, bulk NiO reduced at 500 °C, and NiO prepared by heating $Ni(NO_3)_2$, which is the nickel precursor used in our catalyst preparation, at 500 °C. The three NiO spectra presented in Figure 3 show very similar features which can be identified with Ni^{2+} in NiO species,[28] with Ni $2p_{3/2}$ binding energies appearing at 853.3 eV. The strong shake-up line that appears at 860.8 eV is characteristic of Ni^{2+} species. When NiO samples are reduced at 500 °C, the shake-up lines disappear and the prominent binding energies become 852.4 for Ni 2p3/2, signaling the formation of metallic Ni species.

The other reference spectrum in Figure 3 is that of $NiMoO_4$. Although the characteristic shake-up lines for Ni^{2+} species are clearly visible, the Ni 2p binding energies (855.5 eV for $2p_{3/2}$) are quite distinct from those seen in NiO samples. When this sample is reduced at 500 °C, the shake-up lines disappear and the peak position for the main feature shifts to a lower binding energy of 852.7 eV. This value, although much lower than that of the $NiMoO_4$ and of NiO, is not as low as the metallic Ni binding energy observed over the reduced NiO sample.

The Ni 2p regions of the spectra for the same catalyst samples that are discussed in Figure 2 are presented in Figure 4. The oxidic form of Ni−Mo/Al_2O_3 (O-500) catalyst shows Ni $2p_{3/2}$

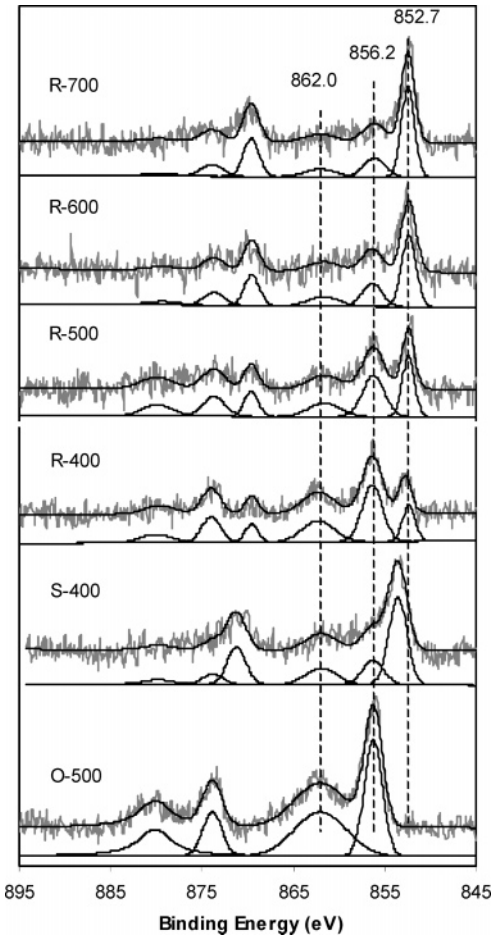

Figure 4. X-ray photoelectron spectra (Ni 2*p* region) of Ni−Mo/Al_2O_3 catalysts reduced at different temperatures. Calcined and sulfided samples are included for comparison.

and $2p_{1/2}$ binding energies at 856.2 and 873.8 eV, respectively, which could be characteristics of Ni_2O_3, $NiAl_2O_4$, or $NiMoO_4$ phases. This sample does not exhibit any features below 856 eV. Although the absence of any peaks below 856 eV in our oxidized catalyst sample leads us to conclude that NiO is not present on the surface in any substantial quantity, the strong shake-up lines at 862.0 and 880.1 eV suggest the presence of Ni^{2+} species, which may be $NiAl_2O_4$ or $NiMoO_4$ species. Kim and Davis[34] reported the presence of satellite peaks in the same region from a Ni_2O_3 phase; however, the relative intensity they reported was significantly lower than what is seen in our samples. Hercules and co-workers, citing the above-mentioned reference, attributed the presence of satellite peaks to Ni_2O_3 in their NiW samples.[35]

The Ni 2p spectrum of the sulfided Ni−Mo/Al_2O_3 catalyst shows two major peaks at 853.5 and 871.1 eV, which are believed to be due to a Ni−Mo−S structure. The fwhm observed for these species (2.3 eV) is smaller than that of the Ni oxide species (2.6 eV). A similar observation was noted for the Mo

TABLE 3: Surface Atomic Ratios of Mo/Al, Ni/Al, and Ni/Mo of Ni−Mo/Al_2O_3 Catalysts Pretreated at Different Conditions

pretreatment	A_{mo}/A_{Al} ($\times 10^2$)	A_{Ni}/A_{Al} ($\times 10^2$)	A_{Ni}/A_{Mo}
as prepared	6.5	2.5	0.39
TEM/EDX	6.6	2.6	0.40
O-500	13.2	3.9	0.30
S-400	9.4	3.6	0.38
R-400	11.2	3.4	0.30
R-500	9.5	2.9	0.31
R-600	8.2	2.7	0.33
R-700	7.6	2.8	0.36

3d binding energies of the oxide versus sulfide species and was explained by the increased conductivity of the sulfided sample as compared to that of the oxidized sample. Deconvolution results (Table 2) show that about 25% of Ni is not sulfided, as seen by the shoulders at 856.2 and 873.8 eV.

The major XPS features for Ni−Mo/Al_2O_3 reduced at 400 °C are at 856.2 and 873.8 eV for Ni $2p_{3/2}$ and Ni $2p_{1/2}$ binding energies, respectively, with strong shake-up lines at 862.0 and 880.1 eV, the same as the oxidized catalyst. A new phase begins to emerge with Ni $2p_{3/2}$ and Ni $2p_{1/2}$ binding energies 852.7 and 870.3 eV and with lower fwhm (1.6 eV). A similar binding energy was observed over the reduced $NiMoO_4$ sample (Figure 3). This binding energy is slightly higher than what is observed for a bulk metallic nickel sample observed by reducing NiO at 500 °C (Figure 3). It is conceivable that these Ni species exist as part of a Ni−Mo−O structure analogous to a Ni−Mo−S structure. With increasing reduction temperature, intensities of the peaks at 852.7 and 870.3 eV increase while those at 862.0 and 880.1 eV decrease. However, the shoulders at 856.2 and 873.8 eV are still apparent, even for the catalyst reduced at 700 °C. The satellite peak at 862.0 eV implies that oxygen ligands attached to nickel still exist. Deconvolution results show that about 26% (Table 2) Ni species are still in an oxidized state (856.2 eV)). This amount is the same as the percentage of Ni species left unsulfided on the "sulfided" sample. It is interesting that the percentage of Ni that cannot be reduced or sulfided is about the same. This value (∼25%) is also very close to what was reported by Ng and Hercules[35] on Ni−W/Al_2O_3 catalyst. It is possible that the percentage of Ni which cannot be reduced or sulfided belongs to a Ni aluminate phase. This finding is in agreement with the "surface spinel" model proposed by Jaccono et al.[36] where Ni^{2+} ions occupy the tetrahedral sites in γ-Al_2O_3. The presence of Co species that cannot be sulfided were also reported for Co−Mo/Al_2O_3 catalysts.[37,38]

The atomic ratios of Mo/Al, Ni/Al, and Ni/Mo, calculated from XPS data, are presented in Table 3. As expected, the Mo/Al and Ni/Al ratios over the oxidized catalyst are higher than the "as prepared" values, showing a higher surface concentration for Mo and Ni. The Mo/Al ratio decreases when the catalyst is sulfided, possibly due to aggregation and "stacking" of Mo in the form of MoS_2. The Ni/Mo ratio, on the other hand, increases, possibly because of the surface decoration of Ni on the edges of the MoS_2 slabs. With increasing reduction temperature, Mo/Al atom ratios decrease gradually, suggesting aggregation and crystallization of Mo species. The decrease in the Ni/Al ratio at lower reduction temperatures may be the result of Ni migration to the bulk to form $NiAl_2O_4$ or may be due to increased alumina surface area that is exposed. At higher reduction temperatures, the Ni/Al ratio remains the same or slightly increases. Since there is more Al surface exposed at these temperatures due to Mo species crystallization, this implies a net increase in Ni surface concentration. It is conceivable that Ni diffuses from the bulk to the surface at higher reduction temperatures, as indicated by Ng and Hercules[35] for the Ni−W/Al_2O_3 catalyst.

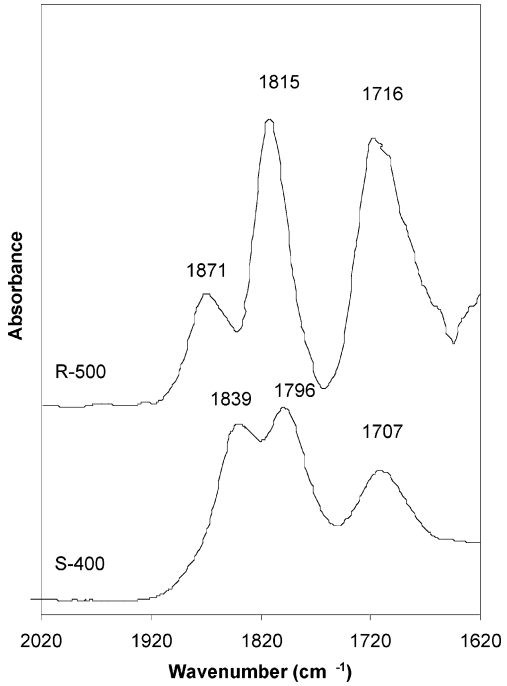

Figure 5. DRIFT spectra of NO adsorbed on reduced and sulfided Ni−Mo/Al_2O_3 catalysts.

3.3. DRIFT Spectra of Probe Molecules. *Adsorption of NO and CO_2.* Figure 5 shows spectra taken over sulfided and reduced NiMo catalysts following NO adsorption. As identified earlier,[21,48] 1707 and 1796 cm^{-1} bands observed over the sulfided sample result from NO adsorption on Mo species, whereas the 1839 cm^{-1} band is associated with the Ni species. The reduced sample also exhibits three features, those at 1716 and 1815 cm^{-1} resulting from Mo species and the one at 1871 cm^{-1} from Ni-related sites. As pointed out in the literature,[5,39] the lower frequencies observed for the sulfided catalyst in comparison to the reduced catalyst are due to increased electron density at the adsorbing metal sites when neighboring O atoms are replaced by less electronegative S atoms.

Figure 6 shows the DRIFT spectra obtained following NO adsorption over samples that are reduced at different temperatures. There is very little NO adsorption over the sample reduced at 250 °C. The intensity of the adsorbed NO bands associated with Ni sites (1871 cm^{-1}) increases with an increase in reduction temperature. This result is consistent with the controlled-atmosphere XPS data, which showed an increase in the peak intensity of the binding energy at 852.7 eV, which is believed to be due to Ni sites in a Ni−Mo−O matrix. The fact that there was no metallic Ni formation observed through XPS or in-situ XRD, even when the reduction temperature was raised to 800 °C, suggests that Ni-associated anion vacancies keep increasing without fully reducing Ni sites to the metallic form. The intensities of the NO bands associated with Mo sites (1815 and 1716 cm^{-1}) also increase with an increase in reduction temperature up to 500 °C. Further increases in reduction temperature, however, cause a decrease in the intensity of these bands. Up to 500 °C, increasing the reduction temperature increases the number of anion vacancies associated with both Ni and Mo sites. At reduction temperatures above 500 °C, however, metallic molybdenum begins to form, decreasing the NO adsorption sites. This observation is consistent with the controlled-atmosphere XPS and in-situ XRD results, which

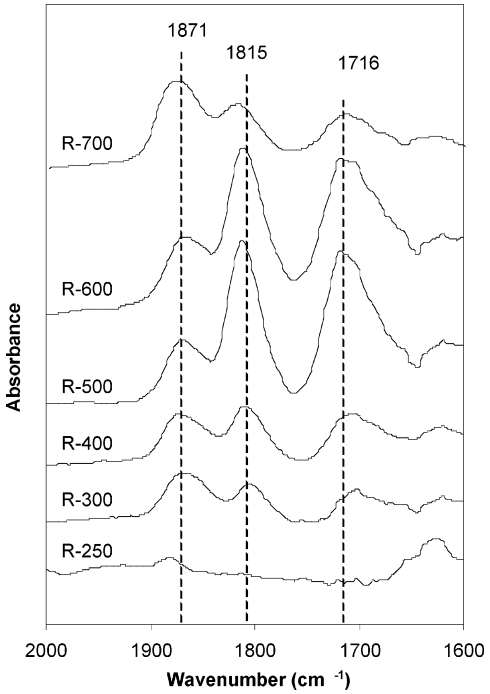

Figure 6. DRIFT spectra of NO adsorbed on Ni−Mo/Al_2O_3 catalysts reduced at different temperatures.

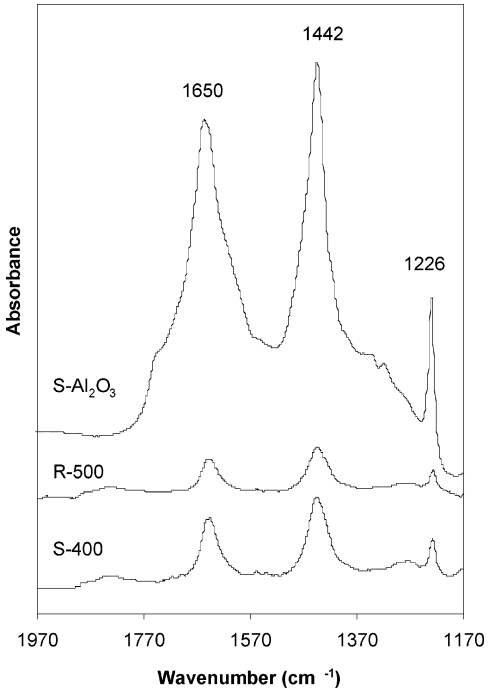

Figure 7. DRIFT spectra of CO_2 adsorbed on reduced and sulfided Ni−Mo/Al_2O_3 catalysts. Sulfided Al_2O_3 support is included for comparison.

showed the presence of metallic Mo in the samples reduced above 500 °C.

Figure 7 shows that the DRIFT spectra taken over the sulfided and reduced samples after CO_2 adsorption are essentially identical. The fact that the band positions are the same as those observed over the sulfided Al_2O_3 support gives support to our assertion that the adsorbed CO_2 bands over these catalysts arise from the Al_2O_3 surfaces left exposed after reduction or sulfidation.

Pyridine Adsorption. Figure 8 shows the adsorbed pyridine bands (adsorbed at 150 °C, followed by flushing with He at

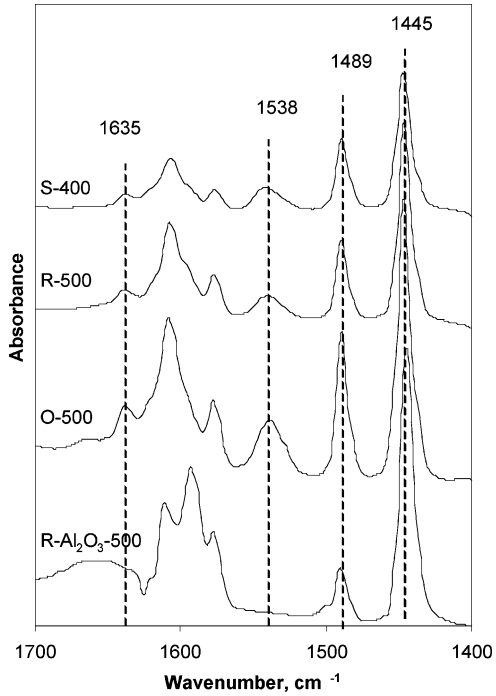

Figure 8. DRIFT spectra of pyridine adsorbed on Ni−Mo/Al_2O_3 samples pretreated at different conditions.

the same temperature) over oxidized (O-500), reduced (R-500), and sulfided (S-400) samples. The spectrum taken over the bare support "reduced" at 500 °C (R-Al_2O_3-500) is also included for comparison.

The bands at 1445 and 1538 cm^{-1} are the characteristics of anti-symmetric vibrations of adsorbed pyridine over L and B acidic sites, respectively. The band at 1489 cm^{-1} has contributions from the symmetrical vibrations of both L and B sites. The band around 1610 cm^{-1} may have contributions from the total symmetric vibration of pyridine on L sites, pyridine adsorbed via hydrogen bonding, and the anti-symmetric vibration in the plane of pyridine on B sites.[49] The band around 1575 cm^{-1} is likely to be from the anti-symmetric vibration in the plane of pyridine on L sites. The shoulder at around 1592 cm^{-1} can be assigned to symmetric vibration of pyridine on L sites. The Al_2O_3 support that went through the reduction step shows strong bands from Lewis acid sites only. No Brønsted acid sites are observed over the bare support. The oxidized sample exhibits strong bands at 1538 and 1635 cm^{-1} (anti-symmetric and symmetric vibration of adsorbed pyridine over Brønsted acidic sites, respectively), signaling the presence of Brønsted acid sites. The spectra taken over the reduced and sulfided samples are very similar, with strong bands arising from pyridine adsorbed on Lewis acid sites along with relatively weak bands from pyridine adsorbed on Brønsted acid sites. One interesting point to note about these results is that pyridine adsorption on Brønsted acid sites over these catalysts was not observed by some researchers, especially when the IR spectra were collected under high vacuum.[40−45] Other researchers, however, reported the presence of Brønsted acid sites in IR spectra as identified by pyridine adsorption,[46,47] in agreement with our observations. The fact that the DRIFT spectra in our experiments were collected without evacuating the sample chamber and by using a high-sensitivity MCT detector (operated at 77 K) can explain why the Brønsted acid sites were clearly visible. It is conceivable that under vacuum conditions, SH^- or OH^- groups may reassociate with H^+ ions and desorb, eliminating the Brønsted acid sites. High-temperature flushing of the sulfided catalyst

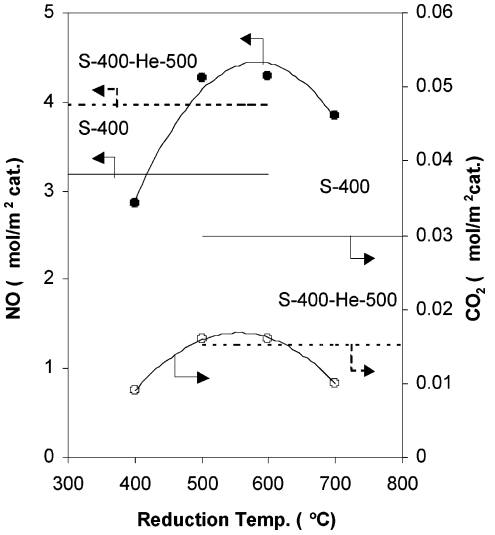

Figure 9. Effect of reduction temperature on NO and CO_2 chemisorption capacities over reduced Ni−Mo/Al_2O_3 catalysts. The values for sulfided samples (represented as straight lines) are included for comparison.

may also have the same effect, since the sulfided Ni−Mo/Al_2O_3 catalyst which was flushed at 500 °C, did not show any Brønsted acid sites in our DRIFTS experiments.[22] The fact that the Brønsted acid sites were observed over both reduced and sulfided catalysts seems to support our earlier assertion that the two catalysts may have analogous sites in the form of OH− and SH− groups or S or O vacancies.[18]

3.4. Volumetric Measurement of Adsorbed Probe Molecules.

Since our previous studies[21,22] over the sulfided catalysts established correlations between the aldehyde hydrogenation activity and NO adsorption capacity as well as between heavy-product formation activity and CO_2 adsorption capacity, similar studies were performed over the reduced catalysts. Figure 9 shows variation of CO_2 and NO adsorption capacities with reduction temperature. The volumetric measurements of CO_2 chemisorption were carried at 30 °C. NO chemisorption was performed at −78 °C to avoid the oxidation−reduction between the surface and the NO molecules. For comparison, the data for the sulfided sample (S-400) and the sample sulfided and then flushed at 500 °C (S-400-He-500) are also included in the figure as solid and dotted lines, respectively.

The CO_2 uptake goes through a maximum with temperature over the reduced catalyst. There are two different factors in operation here that lead to this behavior. On one hand, with an increase of reduction temperature, the exposed Al_2O_3 surface increases because of the aggregation of Mo and Ni species. On the other hand, the amount of OH groups on the Al_2O_3 surface decreases with increasing temperature, due to dehydration, causing a decrease in CO_2 adsorption capacity.

Sulfided catalysts shows a much higher CO_2 adsorption capacity than reduced catalysts. After flushing with He at 500 °C, however, the amount of adsorbed CO_2 for the sulfided catalyst is very close to that for the catalyst reduced at 500 °C. As discussed previously,[22] this may be due to dehydration of the surface and loss of OH groups during the high-temperature flushing.

The NO uptake also goes though a maximum over the reduced catalyst. With increasing reduction temperature, the amount of oxygen anion vacancies associated with Mo and Ni sites increases. However, higher reduction temperatures cause further decrease in the CUS sites by producing metallic Mo species, which do not adsorb NO. The volumetric chemisorption results are consistent with the DRIFT data presented in the previous section.

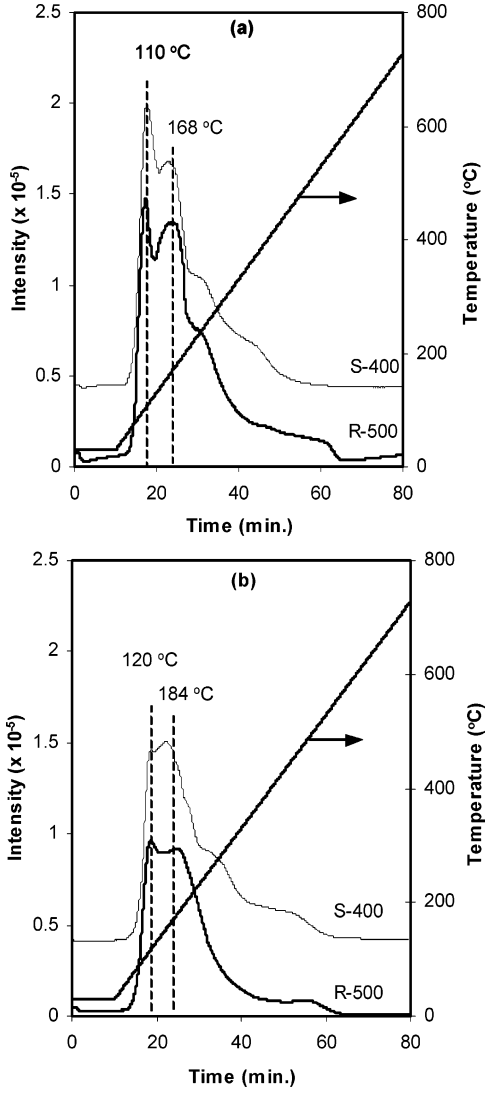

Figure 10. Propanal TPD profiles over reduced and sulfided Ni−Mo/Al_2O_3 catalysts. (a) propanal. (b) 2-methyl-pentenal.

The NO adsorption capacity of the sulfided catalyst is much lower than that of the reduced catalyst. The high-temperature flushing with He improves the NO adsorption capacity of the sulfided catalyst, since H_2S desorption that takes place during the high-temperature flushing step leaves behind additional S anion vacancies. However, the NO adsorption does not reach the levels obtained over the catalyst reduced at the 500−600 °C range.

3.5. Temperature-Programmed Desorption of Propanal.

Figure 10 shows the desorption profiles obtained over the sulfided and reduced catalysts following propanal adsorption. The propanal desorption profiles (Figure 10a) for the two catalysts are very similar, showing two temperature maxima at 110 and 168 °C, attributed to adsorption on the support and on the catalyst, respectively.[20] The only difference is the relative intensity of these two features, which show a much higher contribution from the support for the sulfided catalyst. There are also shoulders, one at 245 °C over the reduced catalyst and two at 245 and 371 °C over the sulfided catalyst. The 2-methyl-pentenal desorption profiles presented in Figure 10b for the sulfided and reduced samples are also very similar, indicating

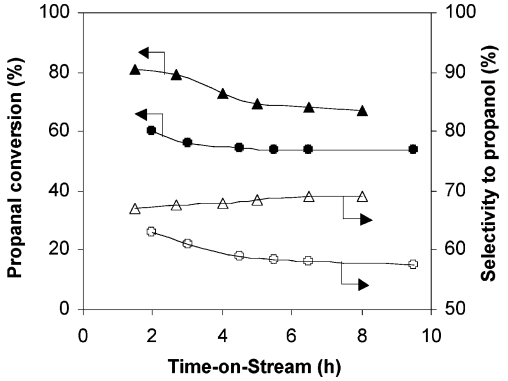

Figure 11. Propanal hydrogenation over reduced and sulfided Ni−Mo/Al_2O_3 catalysts. Reaction conditions: 180 °C, 1000 psi, 0.35% propanal in 250 cm^3 (STP)/min H_2. (●,○) sulfided (400 °C) catalyst; (▲,△) reduced (500 °C) catalyst.

TABLE 4: Product Distribution (% selectivity) in Propanal Hydrogenation over Ni−Mo/Al_2O_3 Catalysts[a]

	180 °C		160 °C		140 °C	
products	S-400	R-500	S-400	R-500	S-400	R-500
propane & ethane	2.8	0.7	1.1	0.2	0.3	0.1
propanol	57.4	69.1	38.6	54.0	29.2	44.6
methyl-pentane (& -pentene)	5.5	4.7	9.0	6.0	9.0	6.4
ethers	2.0	0.9	0.7	0.7	0.4	0.5
propyl acid	0.4	0.4	0.5	0.7	0.6	0.7
2-methyl-pentanal	13.4	7.9	39.8	21.3	49.1	27.4
propyl-propionate	0.5	0.02		0.4		0.4
2-methyl-2-pentenal	0.03	1.0	0.2	12.3	5.6	14.3
acetal	0.03	0.2				
2-methyl-pentanol	12.5	12.3	5.2	3.9	0.7	1.9
2-methyl-pentenol	0.1	0.04	0.2	0.5	0.4	0.5
tri- & tetramers	5.3	2.8	5.3	3.4	5.2	3.4
propanal conversion	53.7	67.0	25.4	40.3	13.6	21.9

[a] Reaction conditions: 1000 psi, 0.35% propanal in 250 cm^3 (STP)/min H_2, 12.5 m^2 catalyst.

that the same types of sites are responsible for the formation of condensation products, such as 2-methyl-pentenal. The only difference is the lower intensity of the peaks observed over the reduced sample, suggesting fewer sites for the formation of heavy products over this catalyst.

3.6. Hydrogenation of Propanal and Hexanal over Ni−Mo/Al_2O_3 Catalysts.

Figure 11 and Table 4 present the results of propanal hydrogenation over reduced and sulfided Ni−Mo/Al_2O_3 catalysts. As seen in Figure 11, propanal hydrogenation over both reduced and sulfided catalysts reaches steady state after 5 h on-stream. Reduced catalyst is seen to be more active for propanal conversion and also has a higher selectivity to propanol than the sulfided catalyst. The apparent activation energies for reduced and sulfided catalysts calculated using the Arrhenius plots are 12 and 15 kcal/mol, respectively. Table 4 presents a comparison of the product distributions for the reduced and sulfided catalysts in the 140−180 °C temperature range. At every temperature, the reduced catalyst has a higher conversion and higher propanol selectivity than the sulfided catalyst. The selectivity to heavy products, on the other hand, is consistently higher over the sulfided catalysts.

Conversion and selectivity data from hexanal hydrogenation over reduced and sulfided Ni−Mo/Al_2O_3 catalysts are presented in Figure 12. In the temperature range of 140 to 180 °C, reduced and sulfided catalysts show the same trends, that is, hexanal conversion and selectivity to hexanol and light products increase with increasing temperature, while selectivity to heavy products

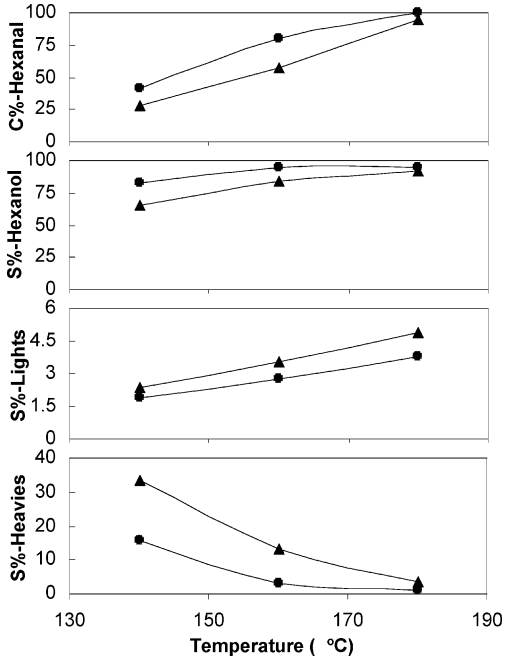

Figure 12. Conversion and selectivity in various products from hexanal hydrogenation over reduced and sulfided Ni−Mo/Al_2O_3 catalysts at different temperatures. Reaction conditions: 1000 psi, 0.09% hexanal in 250 cm^3 (STP)/min H_2. (●) reduced catalyst, (▲) sulfided catalyst.

decreases. The conversion and selectivity to hexanol are higher over the reduced catalyst, while the selectivities to lights and heavies are higher over the sulfided catalysts. The apparent activation energies for hexanal hydrogenation are very similar to those calculated for propanal hydrogenation, with the reduced catalyst showing a somewhat lower activation energy than the sulfided catalyst (13 and 15 kcal/mol, respectively).

Reaction studies with hydrogenation of propanal and hexanal agree closely with the findings from the characterization experiments. Reduced catalysts have higher aldehyde hydrogenation activity than sulfided catalysts. This is consistent with the NO adsorption experiments, which showed a higher abundance of anion vacancies over the reduced catalyst. Similarly, the observation that smaller amounts of heavy products are produced over the reduced catalyst agrees with the chemisorption experiments, which showed a smaller CO_2 adsorption capacity for the reduced catalysts. It needs to be pointed out that sulfided catalysts show a much higher selectivity to 2-methyl-pentanal than reduced catalyst, whereas its selectivity for 2-methyl-pentenal is lower. It may imply that sulfided catalyst can hydrogenate the C═C double bonds more easily while reduced catalyst possesses a higher hydrogenation activity for the C═O double bonds.

4. Summary

Reduced Ni−Mo/Al_2O_3 catalysts show superior aldehyde hydrogenation activity and alcohol selectivity than sulfided catalyts. As shown earlier,[18] reduced catalysts, which may be represented as a Ni−Mo−O structure, possess catalytic behavior analogous to that of Ni−Mo−S catalysts. A reduction temperature of 500 °C appears to be optimum for forming a catalyst surface where the majority of Mo species are in a +4 oxidation state and the oxygen anion vacancies are maximized. This temperature also appears to be optimum for minimizing the exposed alumina surface and the OH groups that lead to heavy-product formation. The in-situ X-ray diffraction, controlled-

atmosphere XPS, DRIFTS, and chemisorption studies have provided complementary data that support this assertion.

References and Notes

(1) Topsøe, H.; Clausen, B. S. *Catal. Rev.—Sci. Eng.* **1984**, *26*, 395.
(2) Topsøe, H.; Clausen B. S.; Candia, R.; Wivel, C.; Morup, S. *J. Catal.* **1981**, *68*, 433.
(3) Wivel, C.; Candia, R.; Clausen, B. S.; Morup, S.; Topsøe, H. *J. Catal.* **1984**, *87*, 497.
(4) Topsøe, H.; Clausen, B. S. *Appl. Catal.* **1986**, *25*, 273.
(5) Topsøe, N.-Y.; Topsøe, H. *J. Catal.* **1983**, *84*, 386.
(6) Topsøe, H.; Clausen, B. S.; Massoth, F. E. *Hydrotreating Catalysis*; Springer-Verlag: Berlin, 1996.
(7) Ho, T. C. *Catal. Rev.—Sci. Eng.* **1988**, *30*, 117.
(8) Satterfield, C. N. *Heterogeneous Catalysis in Industrial Practice*, 2nd ed.; McGraw-Hill: New York, 1991.
(9) Girgis, M. J.; Gates, B. C. *Ind. Eng. Chem. Res.* **1991**, *30*, 2021.
(10) Perot, G. *Catal. Today* **1991**, *10*, 447.
(11) Laurent, E.; Delmon, B. *J. Catal.* **1994**, *146*, 281.
(12) Prins, R. Hydrodesulfurization, hydrodenitrogenation, hydrodeoxygenation, and hydrodechlorination. In *Handbook of Heterogeneous Catalysis*; Ertl, G., Knozinger, H., Weitkamp J., Eds.; VCH: Weinheim, Germany, 1997.
(13) Kim, S. C.; Massoth, F. E. *Ind. Eng. Chem. Res.* **2000**, *39*, 1705.
(14) Zhang, L.; Karakas, G.; Ozkan, U. S. *J. Catal.* **1998**, *178*, 457.
(15) Bunch, A.; Zhang, L.; Karakas, G.; Ozkan, U. S. *Appl. Catal.* **2000**, *190*, 51.
(16) Furimsky, E. *Appl. Catal.* **1983**, *6*, 159.
(17) Vogelzang, M. W.; Li, C. L.; Schuit, G. A.; Gates, B. C.; Petrakis, L. *J. Catal.* **1983**, *84*, 170.
(18) Bunch, A. Y.; Ozkan, U. S. *J. Catal.* **2002**, *206*, 177.
(19) Wang, X.; Li, G.; Ozkan, U. S. *J. Mol. Catal.* **2004**, *217*, 219.
(20) Wang, X.; Saleh, R. Y.; Ozkan, U. S. *J. Catal.*, submitted.
(21) Wang, X.; Ozkan, U. S. *J. Catal.* **2004**, *227*, 492.
(22) Wang, X.; Ozkan, U. S. *J. Mol. Catal.*, submitted.
(23) Ozkan, U. S.; Ni, S.; Zhang, L.; Moctezuma, E. *Energy Fuels* **1994**, *8*, 249.
(24) Ozkan, U. S.; Zhang, L.; Ni, S.; Moctezuma, E. *J. Catal.* **1994**, *148*, 181.
(25) Ozkan, U. S.; Cai, Y.; Kumthekar, M. W.; Zhang, L. *J. Catal.* **1993**, *142*, 182.
(26) Zingg, D. S.; Makovsky, L. E.; Tischer, R. E.; Brown, F. R.; Hercules, D. M. *J. Phys. Chem.* **1980**, *84* (4), 2898.
(27) Li, C. P.; Hercule, D. M. *J. Phys. Chem.* **1984**, *88* (8), 456.
(28) Moulder, J. F.; Stickle, W. F.; Sobol, P. E.; Bomben, K. D. *Handbook of X-ray Photoelectron Spectroscopy*; Chastain, J., Ed.; Perkin-Elmer Corporation: Minnesota, 1992.
(29) Nakamura, R.; Bowman, R. G.; Burwell, R. L. *J. Am. Chem. Soc.* **1981**, *103*, 674.
(30) Yao, H. C. *J. Catal.* **1981**, *70*, 440.
(31) Nakamura, R.; Pioch, D.; Bowman, R. G.; Burwell, R. L. *J. Catal.* **1985**, *93*, 338.
(32) Holl, Y.; Touroude, R.; Marire, G.; Muller, G.; Engelhard, P. A.; Grosmangin, J. *J. Catal.* **1987**, *104*, 202.
(33) Yamada, M.; Yasumaru, J.; Houalla, M.; Hercules, D. M. *J. Phys. Chem.* **1991**, *95*, 7037.
(34) Kim, K. S.; Davis, R. E. *J. Electron Spectroscopy under Related Phenomena* **1972/1973**, *1*, 251.
(35) Ng, K. T.; Hercules, D. M. *J. Phys. Chem.* **1976**, *80*, 2094.
(36) Jacono, M. L.; Schiavello, M.; Cimino, A. *J. Phys. Chem.* **1971**, *75*, 1044.
(37) Brinen, J. S.; Armstron, W. D. *J. Catal.* **1978**, *54*, 57.
(38) Portela, L.; Grange, P.; Delmon, B. *J. Catal.* **1995**, *156*, 243.
(39) Okamoto, Y.; Katoh, Y.; Mori, Y.; Imanaka, T.; Teranishi, S. *J. Catal.* **1981**, *70*, 445.
(40) Segawa, K.; Hall, W. K. *J. Catal.* **1982**, *76*, 133.
(41) Valyon, J.; Schneider, R. L.; Hall, W. K. *J. Catal.* **1984**, *85*, 277.
(42) Suarez, W.; Dumesic, J. A.; Hill, C. G. *J. Catal.* **1985**, *94*, 408.
(43) Mone, R. In *Preparation of Catalysts*; Delmon, B., Jacobs, P. A., Poncelet G., Eds.; Elsevier: Amsterdam, 1976; p 381.
(44) Ratnasamy, R.; Knozinger, H. *J. Catal.* **1978**, *54*, 155.
(45) Riseman, S. M.; Bandyopadhyay, S.; Massoth, F. E.; Eyring M. *Appl. Catal.* **1985**, *16*, 29.
(46) Topsøe, N. Y.; Topsøe, H.; Massoth, F. E. *J. Catal.* **1989**, *119*, 252.
(47) Rajagopal, S.; Marzari, J. A.; Miranda R. *J. Catal.* **1995**, *151*, 192.
(48) Portela, L.; Grange, P.; Delmon, B. *Catal. Rev.—Sci. Eng.* **1995**, *37* (4), 699.
(49) Ward, J. W. In *Zeolite Chemistry and Catalysis*; Rabo, J. A., Ed.; ACS Monograph Vol. 171; American Chemical Society: Washington, DC, 1976; p 118.